A Segmentation-Free Approach for Skeletonization of Gray-Scale Images via Anisotropic Vector Diffusion

Zeyun Yu   and   Chandrajit Bajaj

Department of Computer Science, University of Texas at Austin, Austin, Texas 78712, USA
Emails: {zeyun, bajaj}@cs.utexas.edu

Abstract

In this paper we describe a method for skeletonization of gray-scale images without segmentation. Our method is based on anisotropic vector diffusion. The skeleton strength map, calculated from the diffused vector field, provides us a measure of how possible each pixel could be on the skeletons. The final skeletons are traced from the skeleton strength map, which mimics the behavior of edge detection from the edge strength map of the original image. A couple of real or synthesized images will be shown to demonstrate the performance of our algorithm.

1. Introduction

The skeleton is widely recognized as one of the most important shape descriptors in image processing and pattern recognition. Since the first study by Blum [1], the skeletonization of shapes has attracted attentions from many researchers in various fields. Commonly used computational methods for skeleton extraction include topological thinning [2], approaches based on distance maps [3, 4, 5], hierarchical methods based on Voronoi diagrams [6], voxel-coding based methods [7], and some approaches based on physical simulations [8] or curve evolution [9]. However, all of these techniques compute the skeletons from the object's boundaries. In other words, it is a prerequisite that we should first segment the original images into meaningful regions with well-defined boundaries before the above-mentioned approaches could be applied. Unfortunately, efficient and effective segmentation of an arbitrary real-world image still remains an open problem especially with the existence of much noise. In addition, as also mentioned in [16], region segmentation (or edge detection, if applicable) often involves a loss of information, which, as a result, leads to an inaccurate skeletonization of the original images.

The goal of our work in this paper is to compute the skeletons directly from a gray-scale image, without the segmentation (or edge detection) as an intermediate step. The previous efforts on this topic by other authors can be categorized into three approaches. The first one is based on isotropic diffusion, governed by a set of linear PDE's. In [10], Tari *et al.* proposed a method, which extracts the skeletons from a set of level-set curves of the edge strength function of the original image. The edge strength function is calculated by means of a linear diffusion equation. A later paper, by Chung and Sapiro [11], deals with situations where the features (objects) are always brighter or darker than the background. The original image is treated as a 2D function defined over the image domain, and is diffused according to a family of linear erosion/dilation equations. A post-processing step is employed to extract the crest lines of the deformed image, which are taken as the final skeletons.

The second approach is based on scale-space theory [12]. In [13, 14], the authors proposed a method, which extracts the "cores" from the ridges of a medialness function in scale-space. Lindeberg [15] treated the skeletonization (ridge detection) in a similar way to edge detection in scale-space, with automatic scale selection. It has been pointed out that the Gaussian kernels used in scale-space are closely related to the linear diffusion equations when they are applied to the images. Both the isotropic diffusion and the scale-space techniques have the following major drawbacks. First, linear systems often cause feature-blurring and even a loss of information. Second, linear systems may extract the biased skeletons when curvilinear structures are considered and when the contrasts on both sides of the structures are different. The second problem was addressed in details in [17], where special efforts were made to remove the bias of the extracted skeletons.

The third approach dealing with the skeletonization of gray-scale images without segmentation was proposed more recently by Jang and Hong [16]. In their method, a pseudo-distance map is calculated from the original image using a nonlinear governing equation. Although a nonlinear equation was utilized, the results of their method look quite similar to those of linear systems, e.g., Gaussian smoothing, as pointed out by the authors themselves [16]. In addition, it is not clear in [16] whether this method can handle the problem of biased skeletons, as the authors made use of Steger's algorithm [17] to extract the skeletons from a pseudo-distance map. Regardless of these drawbacks, this approach is most related to our algorithm described below.

Hence we shall give additional words in Section 4 to compare this method with ours.

In this paper we propose to compute the skeletons based on *gradient vector diffusion* [20]. We consider a set of anisotropic diffusion equations applied to initial vector fields that are obtained by various ways. A *skeleton strength map*, analogous to the *edge strength function* [10], is calculated from the diffused vector field, and the final skeletons are extracted by tracing the ridges of the skeleton strength map. The *skeleton strength map* gives a measure of how possible each pixel could be on the skeletons. As demonstrated later, the skeleton strength map gives much higher contrast than most methods described above. In addition, the problem of biased skeletons is easily avoided in our approach, due to the anisotropic property of the diffusions.

The rest of this paper is organized as follows. Sections 2 gives a detailed description of our anisotropic vector diffusion. In Section 3, we present the algorithm for skeleton extraction. Section 4 shows some examples of our skeletonization approach. Several interesting issues will also be addressed there. We conclude this paper in Section 5.

2. Gradient Vector Diffusion

In this paper, we restrict ourselves to gradient vector field of the original image, although other types of vector fields still apply in some specific situations. Gradient vector diffusion is commonly used for two purposes. First, it can smooth the noise seen in the given vector field. This property is similar to the various techniques of image smoothing [18, 19]. Second, vector diffusion can make the non-zero vectors propagate toward the areas of zero-vectors. This property is extremely useful for many real-world images, which contain "flat" regions and hence zero gradients.

In [20], the authors described a diffusion technique to smooth gradient vector fields. The gradient vectors are represented by Cartesian coordinates and similar partial differential equations (PDEs) are separately applied to each component of the vectors:

$$
\begin{cases}
\frac{du}{dt} = \mu \nabla^2 u - (u - f_x)(f_x^2 + f_y^2) \\
\frac{dv}{dt} = \mu \nabla^2 v - (v - f_y)(f_x^2 + f_y^2)
\end{cases}
\tag{1}
$$

where $(u, v,)$ is initialized with $\nabla f(x, y)$, and $f(x, y)$ is an edge strength map of the original image; e.g., $f(x, y) = \|\nabla G_\sigma(x, y) * I(x, y)\|^2$, where $G_\sigma(x, y)$ stands for a Gaussian kernel. These diffusion equations are originally used for image segmentation [20]. In case of skeletonization, the initialization of gradient vector fields may vary with different situations, as described in next section.

The above equations obviously are linear or isotropic. It therefore inherits the drawbacks of most linear systems (e.g., blurred maps and biased skeletons). Another way

to diffuse a gradient vector field is based on the polar-coordinate representation of the vectors [22, 23]. The drawback of this method is its computational burden due to the efforts that have to be made to deal with the periodicity of orientation. We propose here another type of partial differential equations for gradient vector diffusion and attempt to address the afore-mentioned problems. The new PDEs are similar to Eq.(1) except that they are now based on anisotropic diffusion:

$$
\begin{cases}
\frac{du}{dt} = \mu \cdot div(g(\alpha) \cdot \nabla u) - (u - f_x)(f_x^2 + f_y^2) \\
\frac{dv}{dt} = \mu \cdot div(g(\alpha) \cdot \nabla v) - (v - f_y)(f_x^2 + f_y^2)
\end{cases}
\tag{2}
$$

where $g(\cdot)$ is a decreasing function and α is the angle between the central vector and the surrounding vectors. For faster implementation, the calculation of the angle between two vectors is usually approximated by the inner-product of two vectors divided by their magnitudes. For instance, we can define $g(\alpha)$ as follows:

$$
g(\vec{c}, \vec{s}) =
\begin{cases}
e^{\kappa \cdot (\frac{\vec{c} \cdot \vec{s}}{\|\vec{c}\| \|\vec{s}\|} - 1)} & if \ \vec{c} \neq 0 \ and \ \vec{s} \neq 0 \\
0 & if \ \vec{c} = 0 \ or \ \vec{s} = 0
\end{cases}
\tag{3}
$$

where κ is a positive constant; $\vec{c}$ and $\vec{s}$ stand for the central vector and one of the surrounding vectors, respectively. In our implementation of 2D images, we consider 4-neighborhood for each pixel.

A study of Eq.(2) would suggest the following: First, its implementation is similar to that of Eq.(1). Hence, the computational time is comparable to the conventional scheme [20]. Secondly, the weighting function $g(\cdot)$ is designed such that the problem of skeleton bias can be easily avoided. This is because the weighting function $g(\cdot)$ is decreasing as the angle between two vectors (the center and the neighbor) increases from 0 to π. If $g(\cdot)$ goes to zero as the angle approaches π, then the vectors from both sides of curvilinear structures would stop on the central lines of the structures regardless of how different the contrasts would be on both sides of the structures. We shall demonstrate such an example in Section 4. Thirdly, Eq.(2) is very similar to the anisotropic diffusion equation of image smoothing, proposed by Perona and Malik [18]. Therefore, we would expect to see something that shows the uniqueness of the anisotropic property of our system, similar to the edge-preserving property as we saw in Perona-Malik model. In fact, the skeleton strength map, as shown later, does demonstrate this unique property.

Finally, it is worthwhile noting that the second terms on the right sides of both Eq.(1) and Eq.(2) are not considered in the rest of this paper, as they were originally used for better segmentation [20], not for skeletonization.

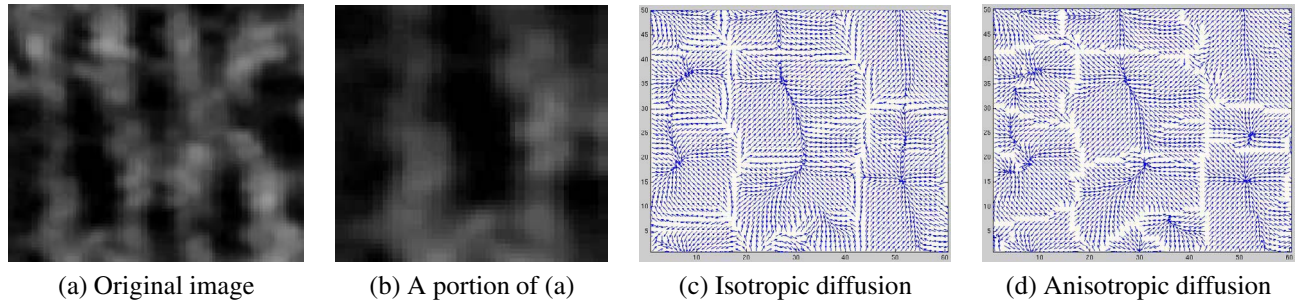|(a) Original image|(b) A portion of (a)|(c) Isotropic diffusion|(d) Anisotropic diffusion|

Figure 1: The demonstration of isotropic and anisotropic vector diffusion schemes on a synthesized molecular image (shown in (a)). For better illustration of vectors, (c-d) are restricted to a portion of the original image, as shown in (b), and all vectors in (c-d) are normalized to the same magnitude.

3. Skeletonization

We describe our skeletonization algorithm step-by-step in the following.

Generation of initial vector field. We first consider images where the objects are brighter than the background. The initial gradient vector field is generated in the following way:

$$gvf(\vec{r}) = (I(\vec{r}) - I(\vec{r'})) \times \frac{\vec{r'} - \vec{r}}{\|\vec{r'} - \vec{r}\|} \qquad (4)$$

where $I(\vec{r})$ is the intensity value at $\vec{r}$. $\vec{r'}$ is one of the (eight) immediate neighbors of $\vec{r}$, with the lowest intensity among the neighbors. Note that this definition of gradient vector is different from other conventional definitions (e.g., the one defined by central difference). We shall see later how Eq.(4) performs better than the conventional definitions.

In case that the objects have lower intensities than the background, the gradient vectors are defined by:

$$gvf(\vec{r}) = (I(\vec{r'}) - I(\vec{r})) \times \frac{\vec{r'} - \vec{r}}{\|\vec{r'} - \vec{r}\|} \qquad (5)$$

where $\vec{r'}$ is one of the (eight) immediate neighbors of $\vec{r}$, with the highest intensity among the neighbors.

Eq.(4) and (5) deal with the situations where the objects are always either brighter or darker than the background. This is the cases discussed in [11]. In general cases [10, 16], one may have to first compute the edge strength map (e.g., $\|\nabla G_\sigma(x, y) * I(x, y)\|$), and then Eq.(5) is applied to the edge strength map to generate the initial vector field.

Gradient vector diffusion. The initial vector field computed above is then diffused using either the isotropic scheme (Eq. (1)) or anisotropic scheme (Eq. (2)). The PDE's are iteratively solved by finite difference technique. In Fig.1(a), we show an example of a synthesized molecular image. In this example, we use Eq.(4) to generate the initial vector field, as the molecular structure is brighter than the background. The diffused vector fields by both isotropic

and anisotropic schemes are shown in Fig.1(c) and Fig.1(d), respectively. For better illustration of vectors, Fig.1(c-d) correspond to only a portion of the original image, as seen in Fig.1(b). We can see that the major difference between these two schemes is that the anisotropic diffusion preserves the "sharp" features (the "blank" regions), where most of the surrounding vectors point away from the central point. A direct observation shows that those features correspond to the skeletons of the original gray-scale image. The superiority of anisotropic diffusion to the isotropic diffusion will be further demonstrated in the following.

Computation of skeleton strength map. To locate the "blank" regions of the diffused gradient vector field, we compute what we call *skeleton strength map* (SSM) by:

$$SSM(\vec{r}) = max(0, \sum_{r' \in N(\vec{r})} \frac{gvf(\vec{r'}) \cdot (\vec{r'} - \vec{r})}{\|\vec{r'} - \vec{r}\|}) \qquad (6)$$

where $N(\vec{r})$ is the set of the eight immediate neighbors of $\vec{r}$. The skeleton strength map, similar to the edge strength map, is a scalar map defined on every pixel and indicates the likelihood of each pixel being on the skeletons. With the original image seen in Fig.1(a), we show in Fig.2(a) the skeleton strength map, generated by anisotropic vector diffusion but initialized by the classical central difference scheme. We can see that this map does not give much clear information on the skeletons of the molecular structures. Fig.2(b) shows the SSM, generated by the isotropic vector diffusion but initialized by Eq.(4). In contrast to the isotropic diffusion technique, Fig.2(c) shows the SSM, generated by anisotropic diffusion and initialized by Eq.(4). A direct comparison between Fig.2(b) and Fig.2(c) would suggest that the isotropic vector diffusion normally tends to blur the skeletons while the anisotropic vector diffusion can preserve the "sharp" skeletons very well. This is analogous to the isotropic/anisotropic diffusion commonly seen in image smoothing [18, 19].
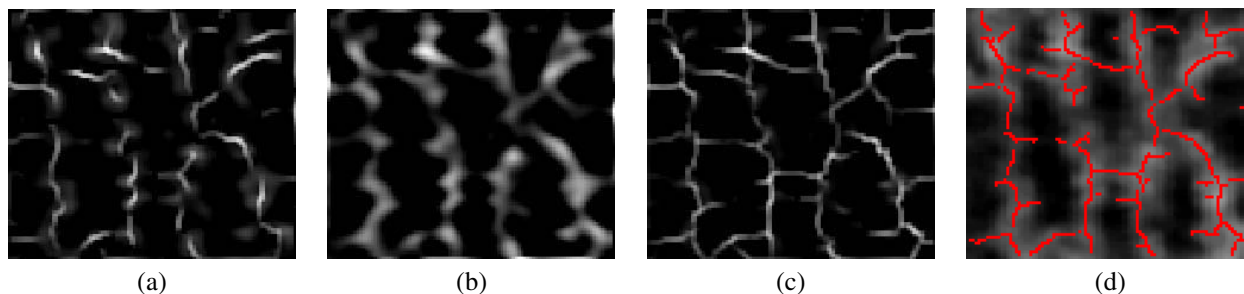
Figure 2: The demonstration of skeleton strength maps skeleton-tracing results. The original image is shown in Fig.1(a). (**a**) SSM by anisotropic vector diffusion, initialized by the classical central difference scheme. (**b**) SSM by isotropic vector diffusion, initialized by Eq.(4). (**c**) SSM by anisotropic vector diffusion, initialized by Eq. (4). (**d**) Skeletons traced from (c).

Skeleton-tracing. To compute the final skeletons, we need to find a way to trace the skeletons from the skeleton strength map. A good technique for this purpose is by Canny's method [21], which was originally designed for image edge detection. The most promising strategies used in this method are non-maximal suppression and double-threshold. The non-maximal suppression is first applied to the gradient magnitude map in order to obtain "thin" edges and extract candidate edges. Two thresholds are assumed such that candidate edges above the higher threshold are always recognized as true edges and candidate edges that are connected to the true edges by a path of pixels with gradient magnitudes higher than the lower threshold are also recognized as true edges. This idea can be readily applied to our skeleton extraction by simply treating the skeletons as the edges. Fig.2(d) shows the skeletons traced by this method from the skeleton strength maps.

4. Results and Discussions

In this section we show several examples and their skeletonization results extracted by our algorithm. Fig.3(a) shows a brain image. Its edge strength map (or gradient magnitude map) is first computed using the derivative of Gaussian kernel function (Fig.3(b)). Eq.(5) is applied to this map to generate an initial vector field, which is then diffused using our anisotropic vector diffusion (Eq.(2)). Ten iterations are applied to solve the PDE (Eq.(2)) using the finite difference scheme. The *skeleton strength map*, shown in Fig.3(c), is calculated from the diffused vector field using Eq.(6). Finally, the skeletons are traced from the skeleton strength map using a modified version of Canny's method.

Fig.4(a) shows another brain image. By the fact that the brain structures have higher intensities than the background, we skip the calculation of the edge strength map, and directly apply Eq.(4) to the original image in order to generate the initial vector field. Our anisotropic vector diffusion scheme (Eq.(2)) is then applied with twenty iterations repeated to solve the PDE. The *skeleton strength map*, shown

in Fig.4(b), is calculated from the diffused vector field using Equation (6), and the final skeletons are shown in Fig.4(c).

The third example that we show here is a binary image consisting of several characters. Although our algorithm is designed for gray-scale images, it can certainly be applied to binary images. Fig.5(a) shows an image of characters. The *skeleton strength map* and the final skeletons are shown in Fig.5(b) and (c), respectively. Note that, since the objects (characters) are darker than the background, we use Eq. (5) to generate the initial vector field and the calculation of edge strength map is skipped. Twenty iterations are applied to solve the PDE (Eq.(2)) using the finite difference scheme.

We mentioned before that the pseudo-distance map (PDM) [16] was most related to our algorithm. In order to see the difference between the PDM and our skeleton strength map (SSM), we consider a simple 1D function, as colored by blue in Fig.6(a). This is a box function with same contrast on both sides. The pseudo-distance map of this function is given by light blue color in Fig.6(a). The skeleton strength maps, generated by isotropic vector diffusion (Eq.(1)) and anisotropic vector diffusion (Eq.(2)), are given by green and red curves, respectively, in Fig.6(a). We can see from this example that our skeleton strength maps give "sharper" ridges. We can also observe that the anisotropic diffusion performs better than the isotropic diffusion.

Finally let us address the bias problem, as we mentioned earlier. For this purpose, we consider a (1D) box function with different contrasts on both sides, as colored by blue in Fig.6(b). The green curve shows the results of our skeleton strength map (anisotropic), from which we can correctly locate the skeleton at the center of the box, as indicated by green arrow in the figure. In contrast, we consider two classical linear methods. One is the direct convolution of a Gaussian kernel with the original data (e.g., see [12, 13, 17]). The result of the convolution is shown by red curve in Fig.6(b). The other linear system, as used in [10], is more general, where the edge strength map is first generated and diffused. The skeletons are then extracted from certain critical points of the diffused edge strength map (e.g., see

[10]). The result of the diffused edge strength map is shown by light blue color in Fig.6(b). From this figure, we can conclude that both linear methods yield biased skeletons, as indicated by red and light blue arrows. The skeletons "shift" to the side with lower contrast. The bias problem was discussed in details in [17], where a lot of efforts have to be made to remove the bias from the extracted skeletons. From the above description, we can see that this problem can be easily solved using our anisotropic vector diffusion.

5. Summary and Conclusion

In this paper we described a skeletonization approach for gray-scale images without any intermediate segmentation step. Our method was based on an anisotropic vector diffusion scheme. We introduced a concept, called *skeleton strength map*, which is analogous to the edge strength map as seen in [10]. Our skeleton strength map gives much "sharper" ridges of the original images than the pseudo-distance map[16]. We also addressed the removal of bias as commonly seen in many linear skeletonization approaches. Our approach for skeleton extraction is treated in a similar way to the edge detection with slight changes.

References

[1] H. Blum, "A Transformation for Extracting New Descriptors of Shape", *Models for the Perception of Speech and Visual Form* (W. Wathen-Dunn, Ed.), MIT Press, pp. 363-380, 1967.

[2] L. Lam, S.W. Lee, and C.Y. Suen, "Thinning Methodologies - A Comprehensive Survey", *IEEE Trans. on Pattern Analysis and Machine Intelligence*, Vol. 14, No. 9, pp. 869-885, 1992.

[3] C. Arcelli and G.S. Baja, "Ridge Points in Euclidean Distance Maps", *Pattern Recognition Letters*, Vol. 13, pp. 237-243, 1992.

[4] R. Kimmel, D. Shaked, N. Kiryati, and A.M. Bruckstein, "Skeletonization via Distance Maps and Level Sets", *Computer Vision and Image Understanding*, Vol. 62, No. 3, pp. 382-391, 1995.

[5] G. Malandain and S.F. Vidal, "Euclidean Skeletons", *Image and Vision Computing*, Vol. 16, No. 5, pp. 317-327, 1998.

[6] R.L. Ogniewicz and O. Kubler, "Hierarchic Voronoi Skeletons", *Pattern Recognition*, Vol. 28, No. 3, pp. 343-359, 1995.

[7] Y. Zhou and A. Toga, "Efficient Skeletonization of Volumetric Objects", *IEEE Transactions on Visualization and Computer Graphics*, Vol. 5, pp. 196-209, 1999.

[8] T. Grogorishin, G. Abdel-Hamid, and Y.H. Yang, "Skeletonization: An Electrostatic Field-Based Approach", *Pattern Analysis and Application*, Vol. 1, No. 3, pp. 163-177, 1996.

[9] K. Siddiqi, S. Bouix, A. Tannenbaum, and S.W. Zucker, "The Hamilton-Jacobi Skeleton", *Proc. Int'l. Conf. Computer Vision*, pp. 828-834, 1999.

[10] S. Tari, J. Shah, and H. Pien, "Extraction of Shape Skeletons from Gray-scale Images", *Computer Vision and Image Understanding*, Vol. 66, No. 2, pp. 133-146, 1997.

[11] D.H. Chung and G. Sapiro, "Segmentation-free Skeletonization of Gray-scale Images via PDE's", *Proc. Int'l Conf. Image Processing*, pp. 927-930, 2000.

[12] T. Lindeberg, *Scale-space Theory in Computer Vision*, The Kluwer International Series in Engineering and Computer Science, Kluwer Academic Publishers, Netherlands, 1994.

[13] S.M. Pizer, D. Eberly, D.S. Fritsch, and B.S. Morse, "Zoom-invariant Vision of Figural Shape: The Mathematics of Cores", *Computer Vision and Image Understanding*, Vol. 69, No. 1, pp. 55-71, 1998.

[14] B.S. Morse, S.M. Pizer, D.T. Puff, and C. Gu, "Zoom-invariant Vision of Figural Shape: Effects on Cores of Images Disturbances", *Computer Vision and Image Understanding*, Vol. 69, No. 1, pp. 72-86, 1998.

[15] Tony Lindeberg, "Edge Detection and Ridge Detection with Automatic Scale Selection", *International Journal of Computer Vision*, Vol. 30, No. 2, pp. 117–154, 1998.

[16] J.H. Jang and K.S. Hong, "A Pseudo-distance Map for the Segmentation-free Skeletonization of Gray-scale Images", *Proc. Int'l Conf. Computer Vision*, pp. 18-23, 2001.

[17] C. Steger, "An Unbiased Detector of Curvilinear Structures", *IEEE Transactions on Pattern Analysis and Machine Intelligence*, Vol. 20, No. 2, pp. 113-125, 1998.

[18] P. Perona and J. Malik, "Scale-Space and Edge Detection Using Anisotropic Diffusion", *IEEE Trans. on Pattern Analysis and Machine Intelligence*, Vol. 12, No. 7, pp. 629-639, 1990.

[19] J. Weickert, *Anisotropic Diffusion In Image Processing*, ECMI Series, Teubner, Stuttgart, ISBN 3-519-02606-6, 1998.

[20] C. Xu and J.L. Prince, "Snakes, Shapes, and Gradient Vector Flow", *IEEE Trans. Image Processing*, Vol. 7, No. 3, pp. 359-369, 1998.

[21] J. Canny, "A Computational Approach to Edge Detection", *IEEE Transactions on Pattern Analysis and Machine Intelligence*, Vol. 8, pp. 679-698, 1986.

[22] Z. Yu and C. Bajaj, "Image Segmentation Using Gradient Vector Diffusion and Region Merging", *Proc. Int'l Conf. Pattern Recognition*, p. 941-944, 2002.

[23] Z. Yu and C. Bajaj, "Anisotropic vector diffusion in image smoothing", *Proc. Int'l Conf. Image Processing*, pp. 828-831, 2002.
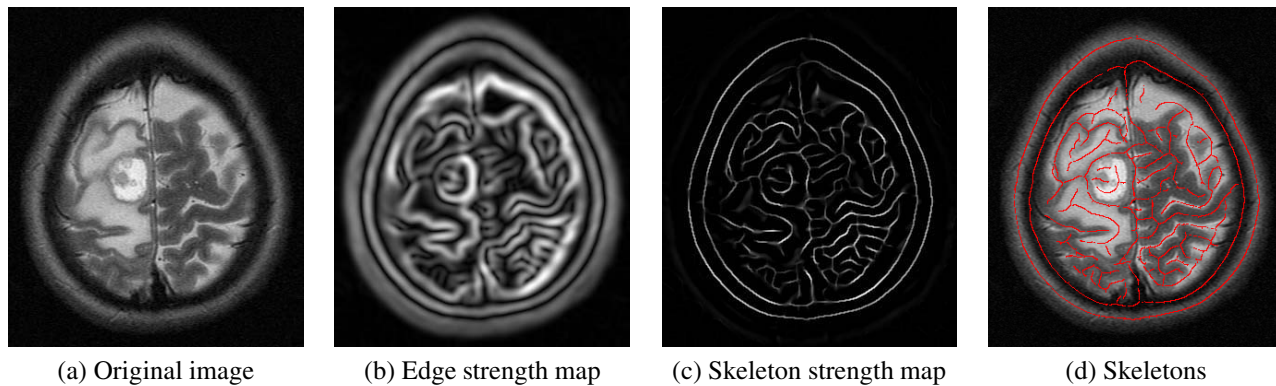
(a) Original image   (b) Edge strength map   (c) Skeleton strength map   (d) Skeletons

Figure 3: The demonstration of skeletonization results (in red color) on a brain MRI data.

(a) Original image   (b) Skeleton strength map   (c) Skeletons
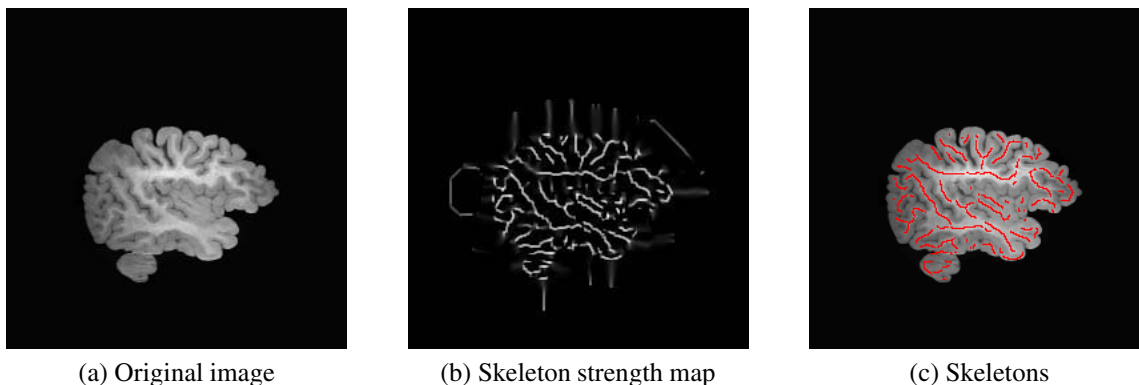
Figure 4: The demonstration of skeletonization results (in red color) on a brain MRI image.
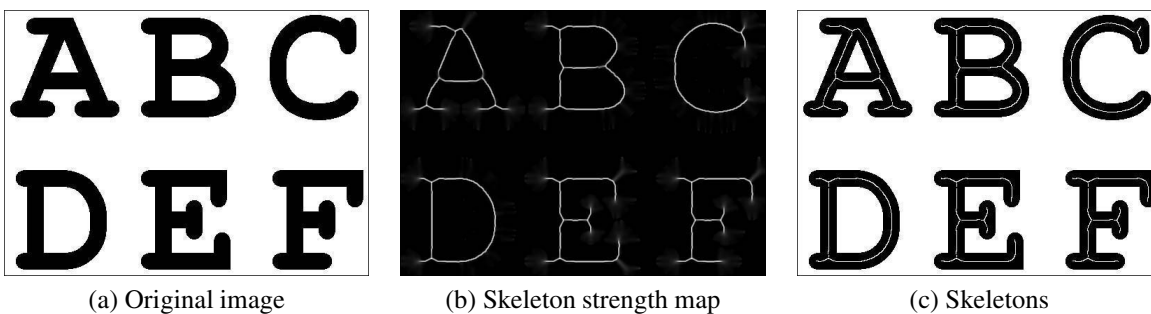

(a) Original image   (b) Skeleton strength map   (c) Skeletons

Figure 5: The demonstration of skeletonization results on an image of several English characters.

(a) Comparison between PDM and SSM   (b) Removal of bias problem by our method

Figure 6: Two tests